

This work was written as part of one of the author's official duties as an Employee of the United States Government and is therefore a work of the United States Government. In accordance with 17 U.S.C. 105, no copyright protection is available for such works under U.S. Law.

Public Domain Mark 1.0

<https://creativecommons.org/publicdomain/mark/1.0/>

Access to this work was provided by the University of Maryland, Baltimore County (UMBC) ScholarWorks@UMBC digital repository on the Maryland Shared Open Access (MD-SOAR) platform.

Please provide feedback

Please support the ScholarWorks@UMBC repository by emailing scholarworks-group@umbc.edu and telling us what having access to this work means to you and why it's important to you. Thank you.



Saturn's magnetosphere interaction with Titan for T9 encounter: 3D hybrid modeling and comparison with CAPS observations

A.S. Lipatov^{a,b,c,d,*}, E.C. Sittler Jr.^b, R.E. Hartle^b, J.F. Cooper^b, D.G. Simpson^b

^a The Goddard Planetary and Heliophysics Institute, University of Maryland, Baltimore County, USA

^b NASA Goddard Space Flight Center, Greenbelt, MD 20771, USA

^c Dialogue-Science, A.A. Dorodnitsyn Computing Center Russian Academy of Science, Vavilov Street 40, 119991 Moscow, Russia

^d Faculty of Problems of Physics and Power Engineering, Moscow Institute of Physics and Technology, Russia

ARTICLE INFO

Article history:

Received 20 September 2010

Received in revised form

23 August 2011

Accepted 31 August 2011

Available online 24 September 2011

Keywords:

Ionospheres

Atmospheres

Induced magnetospheres

Magnetic barrier

Alfvén wing

Plasma modeling

ABSTRACT

Global dynamics of ionized and neutral gases in the environment of Titan plays an important role in the interaction of Saturn's magnetosphere with Titan. Several hybrid simulations of this problem have already been done (Brecht et al., 2000; Kallio et al., 2004; Modolo et al., 2007a; Simon et al., 2007a, 2007b; Modolo and Chanteur, 2008). Observational data from CAPS for the T9 encounter (Sittler et al., 2009) indicates an absence of O^+ heavy ions in the upstream that change the models of interaction which were discussed in current publications (Kallio et al., 2004; Modolo et al., 2007a; Simon et al., 2007a, 2007b; Ma et al., 2007; Szego et al., 2007). Further analysis of the CAPS data shows very low density or even an absence of H^+ ions in upstream. In this paper we discuss two models of the interaction of Saturn's magnetosphere with Titan: (A) high density of H^+ ions in the upstream flow (0.1 cm^{-3}), and (B) low density of H^+ ions in the upstream flow (0.02 cm^{-3}). The hybrid model employs a fluid description for electrons and neutrals, whereas a particle approach is used for ions. We also take into account charge-exchange and photoionization processes and solve self-consistently for electric and magnetic fields. The model atmosphere includes exospheric H^+ , H_2^+ , N_2^+ and CH_4^+ pickup ion production as well as an immobile background ionosphere and a shell distribution for active ionospheric ions ($M_i=28 \text{ amu}$). The hybrid model allows us to account for the realistic anisotropic ion velocity distribution that cannot be done in fluid simulations with isotropic temperatures. Our simulation shows an asymmetry of the ion density distribution and the magnetic field, including the formation of Alfvén wing-like structures.

The results of the ion dynamics in Titan's environment are compared with Cassini T9 encounter data (CAPS).

© 2011 Elsevier Ltd. All rights reserved.

1. Introduction

The interaction of plasma flow with moons and planets is a one of the basic problems of astrophysical plasma due to the complexity of wave-particle processes on multiple time and spatial scales. There are three types of interactions of the solar wind with planets: (a) Earth-like strong interaction; (b) Moon-like weak interaction; (c) Venus-like intermediate interaction. In the last case, the solar wind directly interacts with an ionized planetary environment via the induced magnetic field. In the case

of moons of the outer planets, the mass loading of the magnetospheric plasma by pickup ions, sputtering of fragments from the surface, wave-particle interactions, and inductive magnetic field may play very important role in the interaction of the plasma flow with the moon.

Near Titan, ion reactions such as electron impact ionization, photoionization by the solar EUV flux, and charge exchange (Stebbins et al., 1964) are of significant interest. Wave-particle interactions play a very important role in the possible formation of a shock wave or an Alfvén wing, and in coupling of pickup and upstream ions via excitation of low-frequency waves. These kinetic processes become important in the formation of an obstacle for the upstream flow.

Magnetohydrodynamic (MHD) simulations have been useful for the study of the interaction between plasma flow and Titan (Keller and Cravens, 1994; Ledvina and Cravens, 1998; Cravens et al., 1998; Kabin et al., 1999, 2000; Nagy et al., 2001; Ma et al., 2007). MHD simulations demonstrated a global picture of magnetospheric

* Corresponding author, NASA GSFC, Code 673, Building 21, Room 247, 8800 Greenbelt Road, Greenbelt, MD 20771, USA. Tel.: +1 301 286 0906; fax: +1 301 286 1648.

E-mail addresses: Alexander.Lipatov-1@nasa.gov, alipatov@umbc.edu (A.S. Lipatov), Edward.C.Sittler@nasa.gov (E.C. Sittler Jr.), Richard.E.Hartle@nasa.gov (R.E. Hartle), John.F.Cooper@nasa.gov (J.F. Cooper), David.G.Simpson@nasa.gov (D.G. Simpson).

interaction with a moon, including mass loading the magnetosphere's plasma with the atmosphere's pickup ions and possible chemical processes inside the exobase where the fluid approximation is good. However, several kinetic effects have been lost, namely: asymmetry in the form of an Alfvén wing and a magnetic barrier near a moon, an asymmetry in the atmosphere's pickup ion distribution, possible plasma structure with a thickness of the order of the heavy ion gyroradius, an overestimate of the pickup ion fluxes along the magnetic field, and the absence of the kinetic effects inside plasma structures. Many of these effects may be recovered by using hybrid simulations.

Several 3D hybrid simulations of Titan plasma interactions were performed during the last decade as described in papers by Brecht et al. (2000), Kallio et al. (2004), Sillanpää et al. (2006), Kallio et al. (2007), Modolo et al. (2007a), Simon et al. (2007a, 2007b), and Modolo and Chanteur (2008). The hybrid modeling in Simon et al. (2007a, 2007b) uses a curvilinear grid with a grid spacing about of 772.5 km. In hybrid models by Brecht et al. (2000), Modolo and Chanteur (2008), Sillanpää et al. (2006), Kallio et al. (2007), and Lipatov et al. (2011), they use a rectangular grid with a grid spacing about of 250–500 km. Both Modolo and Chanteur (2008) and Lipatov et al. (2011) use subcycling time integration for the electromagnetic field to avoid a Courant–Friedrich–Levy (CFL) restriction on time step in case of whistler excitation.

These simulations were devoted to an interpretation of Voyager 1 and Cassini data and assumed the presence of the heavy ions like O^+ in magnetospheric plasma. Kallio et al. (2007), discusses hybrid modeling for T9 in the presence of H_2^+ and H_1^+ ions in the upstream flow. However, they used a higher total density (0.4 cm^{-3}) for these ions than was observed in the CAPS T9 measurements (0.05 cm^{-3}) (Sittler et al., 2010). The main results that were obtained in these simulations are the following: asymmetry of a nonstationary bow shock (when Titan's location is outside Saturn's magnetosphere) and the magnetic barrier due to the large gyroradius of magnetospheric ions. Hybrid simulations provided good results for the TA encounter. However, an understanding and interpretation of the CAPS data for the T9 encounter requires models with other upstream environments.

In this paper we discuss two models of the interaction of Saturn's magnetosphere with Titan: (A) high density of H^+ ions in the upstream flow and (B) low density of H^+ ions in the upstream flow. The reason for investigating these models is the uncertainty in the plasma parameters in the upstream flow. The main goal of our paper is to compare these two models of the interaction between Saturn's magnetosphere and Titan.

In our study, the model of the neutral atmosphere has been taken from Hartle et al. (2006) and Sittler et al. (2005). Photoionization, electron impact, and charge exchange rates were taken from Sittler et al. (2005). We apply a time-dependent Boltzmann's "particle in cell" approach (Lipatov et al., 1998), together with a hybrid plasma (ion kinetic) model (Lipatov et al., 2002) in three spatial dimensions (see, e.g., Lipatov and Combi, 2006) using a prescribed but adjustable neutral atmosphere and ionosphere model for Titan. A Boltzmann modeling is applied to model charge exchange between (incoming and pickup) ions and the immobile atmospheric neutrals. In this paper we discuss the results of a hybrid kinetic modeling of Titan's environment, namely, global plasma structures, e.g., the formation of a magnetic barrier, Alfvén wing, pickup ion tail, etc. The results of this kinetic modeling are compared with Cassini T9 flyby observational data (CAPS).

The paper is organized as follows: in Section 2 we present the computational model and a formulation of the problem. In Section 3 we present the results of modeling the plasma environment near Titan and compare with observational data. Finally, in

Section 4 we summarize our results and discuss the future development of our computational model.

2. Formulation of the problem and mathematical model

2.1. Computational model

To study the interaction of Saturn's magnetosphere with the ionized and neutral components of Titan's environment we use a quasineutral hybrid model, namely, a kinetic description for the upstream and pickup ions, and a fluid approximation for electrons. The hybrid model well describes wave–particle interactions on the following ion spatial (λ) and time (ω^{-1}) scales: $\lambda \propto \rho_{ci} = U_0/\Omega_i$ or $\lambda \propto c/\omega_{pi}$ and $\lambda \gg \rho_{ce}$; $\omega \leq \Omega_i$, where ρ_{ci} and ρ_{ce} denote the gyroradius for ions and electrons (respectively); U_0 is the bulk velocity of the upstream flow; c/ω_{pi} denotes the ion inertial length and Ω_i is the ion gyrofrequency. The λ may represent a wavelength of the excited low-frequency waves or a spatial scale of the plasma structures and boundaries in Titan's environment. The model includes photoionization, electron impact ionization and charge exchange. We explicitly include ionization, mass-loading and charge exchange as the dominant mechanisms for the interaction above the lower boundary at Titan. We also include finite conductivity, given by the diffusion scale length, at the inner boundary. The atmosphere is considered to be an immobile component in this paper.

The general scheme of the global interaction of Saturn's magnetosphere with Titan and the Cassini T9 trajectory is given in Fig. 1. The Cassini T9 flyby occurred nearly in the equatorial plane of Titan and perpendicular to the direction of the corotating plasma flow past Titan. The spacecraft trajectory passed approximately 10,768 km ($4.2R_T$) down-stream from Titan (in the sense of the plasma torus flow). Here, R_T denotes the radius of Titan ($R_T = 2575 \text{ km}$). In our coordinate system the x -axis is parallel to U_0 (corotational plasma velocity), y is directed toward Saturn, and z is directed to the north.

In the hybrid model described here, the dynamics of upstream ions and implanted ions is represented with a kinetic approach, while the dynamics of the electrons is described by a hydrodynamical approximation.

The single particle ion distribution function $f_s(t, \mathbf{x}, \mathbf{v})$ has to fulfill the Vlasov/Boltzmann equation:

$$\frac{\partial}{\partial t} f_s + \mathbf{v} \cdot \frac{\partial}{\partial \mathbf{x}} f_s + \frac{\mathbf{F}}{M_s} \cdot \frac{\partial}{\partial \mathbf{v}} f_s = F_{coll} + P - L_{exch}, \quad (1)$$

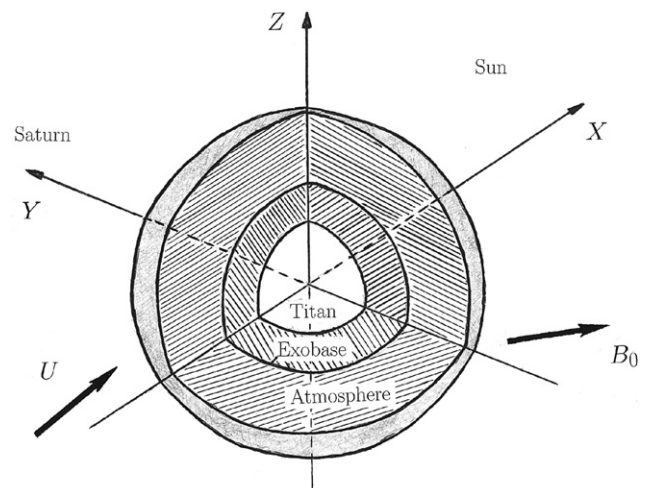


Fig. 1. Titan's plasma environment and the system of coordinates.

where \mathbf{F} symbolizes the Lorentz and gravitation forces, F_{coll} is the collision term, P denotes the production rate of the ions by an ionization and charge exchange, and L_{exch} the loss rate of ions due to charge exchange at (\mathbf{x}, \mathbf{v}) . There are a several computational models to solve Eq. (1): the Vlasov direct methods, particle-in-cell methods, etc. In our paper we use the particle-mesh (PM) model for ion dynamics. Charge-exchange, photoionization, and electron impact were also added to the standard PM technique.

Single ion particle motion is described by the equations (see, e.g., Mankofsky et al., 1987, Eqs. (1) and (14)):

$$\begin{aligned} \frac{d\mathbf{r}_{s,l}}{dt} &= \mathbf{v}_{s,l}, \\ \frac{d\mathbf{v}_{s,l}}{dt} &= \frac{e}{M_s} \left(\mathbf{E} + \frac{\mathbf{v}_{s,l} \times \mathbf{B}}{c} \right) - \frac{m_e v_{se}}{M_s} (\mathbf{v}_{s,l} - \mathbf{U}_i) - \frac{m_e v_{se}}{M_s} \mathbf{J} - v_{so} \mathbf{v}_{s,l}. \end{aligned} \quad (2)$$

Here we assume that the charge state is $Z_i = 1$. \mathbf{U}_i and \mathbf{J} denote the charge-averaged velocity of all (incoming and pickup) ions and the total current (see Eq. (5)). The subscript s denotes the ion population ($s=1$ for incoming ions and $s=2,3,4,5$ for H^+ , H_2^+ , N_2^+ , CH_4^+ pickup ions; $s=6$ for ionospheric ions) and the index l is the particle index. v_{ie} and v_{io} are slowing-down collision frequencies between ions and electrons, and ions and neutrals that may include Coulomb collisions and effects of wave-particle interactions.

In our modeling we use the low (much smaller than the real value) effective conductivity to suppress “shot” noise; hence, we may drop the first collision term in the right hand side of Eq. (2) for simplicity (see Section 2.3). We also drop the third collisional term in Eq. (2), account for the interaction of ions with neutral particles in the region above the exobase and assume that the bulk velocity and temperatures of neutral particles equal zero.

In the nonradiative limit, Ampère’s law is given by

$$\frac{4\pi}{c} \mathbf{J} = \nabla \times \mathbf{B} \quad (3)$$

and the induction equation (Faraday’s law) by

$$\frac{1}{c} \frac{\partial \mathbf{B}}{\partial t} + \nabla \times \mathbf{E} = 0. \quad (4)$$

The total current is given by

$$\mathbf{J} = \mathbf{J}_e + \mathbf{J}_i, \quad \mathbf{J}_i = \sum_{s=1}^{N_{\text{species}}} n_s \mathbf{U}_s = n_i \mathbf{U}_i, \quad (5)$$

where \mathbf{U}_s is the bulk velocity of ions of the type s .

We further assume quasi-neutrality

$$n_e = \sum_{s=1}^{N_{\text{species}}} n_s. \quad (6)$$

In absence of the electron inertia, the equation of motion of the electron fluid takes the form of standard generalized Ohm’s law (e.g., Mankofsky et al., 1987):

$$\mathbf{E} = \frac{1}{en_e c} (\mathbf{J}_e \times \mathbf{B}) - \frac{1}{en_e} \nabla p_e - \frac{m_e}{e} \left[\sum_s v_{es} \left[(\mathbf{U}_i - \mathbf{U}_s) - \frac{\mathbf{J}}{ne} \right] + v_{eo} \mathbf{U}_e \right], \quad (7)$$

where $p_e = nm_e \langle v_e^2 \rangle / 3 = n_e T_e$, and v'_e are the scalar electron pressure and the thermal velocity of electrons; the electron current is estimated from Eq. (5).

Since we suppose that electron heating due to collisions with ions is very small, the electron fluid is considered adiabatic. For simplicity we assume that the total electron pressure may be represented as a sum of partial pressures of all electron populations:

$$p_e = p_{e0} \frac{(\beta_e n_{i,up}^{5/3} + \sum_s \beta_{e,Pl,s} n_{i,Pl,s}^{5/3} + \beta_{e,iono} n_{i,iono}^{5/3})}{\beta_e n_0^{5/3}}, \quad (8)$$

where β_e , $\beta_{e,Pl,s}$, and $\beta_{e,iono}$ denote electron upstream, pickup and ionosphere betas. p_{e0} and n_0 are the upstream electron pressure and ion density. We also assume that $n_{e,up} = n_{i,up}$, $n_{e,Pl,s} = n_{i,Pl,s}$, and $n_{e,iono} = n_{i,iono}$. Here, $n_{i,iono}$ denotes the immobile ionosphere ions. Otherwise, we have to calculate the electron pressure from heat balance for electrons (see, e.g., Braginskii, 1965) taking into account the heat fluxes for pickup electrons and ionospheric electrons on the right side of this equation. The ion kinetic approach allows us to take into account the effects of anisotropy of ion pressure, the correct mass loading processes, the penetration of ions across the ionosphere, and the asymmetry of plasma flow around Titan.

Neutral atmosphere: The neutral atmosphere of Titan serves as a source of new ions, mainly by electron impact ionization with the magnetospheric plasma and by photoionization. Particles of the neutral atmosphere also serve as collisional targets for charge exchange with magnetospheric protons.

We have adopted a four-species description for the neutral exosphere of Chamberlain’s form, the product of the barometric density

$$n_{\text{neutral},k}(r) = n_{\text{atmos},k} \exp(-(1/r - 1/r_{\text{exobase}}) h_{\text{atmos},k}) \quad (9)$$

and the partition function (see, e.g., Amsif et al., 1997; Sittler et al., 2010, Figure 18). In Eq. (9), index k denotes H , H_2 , CH_4 , and N_2 , and their maximum values of the neutral density extrapolated to the exobase are $n_{\text{atmos},\text{H}} = 2.0 \times 10^4 \text{ cm}^{-3}$, $n_{\text{atmos},\text{H}_2} = 2.0 \times 10^5 \text{ cm}^{-3}$, $n_{\text{atmos},\text{CH}_4} = 1.2 \times 10^6 \text{ cm}^{-3}$ and $n_{\text{atmos},\text{N}_2} = 1.2 \times 10^7 \text{ cm}^{-3}$ (Yelle et al., 2006). The radius of the exobase is $r_{\text{exobase}} \approx 4000 \text{ km}$. Their spatial scales are $h_{\text{atmos},\text{H}} = 2.2 \times 10^4 \text{ km}$, $h_{\text{atmos},\text{H}_2} = 2.75 \times 10^4 \text{ km}$, $h_{\text{atmos},\text{CH}_4} = 8.3 \times 10^4 \text{ km}$ and $h_{\text{atmos},\text{N}_2} = 1.77 \times 10^5 \text{ km}$. The thermal velocity of all newly formed pickup ions is about 0.25 km/s .

Ionosphere: We use a model of the ionosphere that contains a shell-like immobile ionosphere at the Sun side at $R_{\text{iono}} = 1300 \text{ km} + R_T$:

$$n_{\text{iono}} = n_{\text{iono},R_{\text{iono}}} \exp(-(r - R_{\text{iono}})^2 / \delta_{\text{iono}}^2) \quad (10)$$

and simulate the ionospheric ion flux using active ion macro-particles with $M_i = 28 \text{ amu}$:

$$\text{flux}_{\text{iono}} = \text{flux}_{\text{iono},R_{\text{iono}}} \exp(-(r - R_{\text{iono}})^2 / \delta_{\text{iono}}^2). \quad (11)$$

Here $\delta_{\text{iono}} = 200 \text{ km}$ is a characteristic spatial scale for the thickness of the ionosphere, and the total flux through ionosphere is about $5 \times 10^{25} \text{ ion/s}$. Initially the thermal velocity of active ion macro-particles is about 0.25 km/s . Note that an immobile ionosphere with a density $n_{\text{iono},R_{\text{iono}}} = 6.25 \text{ ion/cm}^3$ is used in the modeling to avoid a low value of density due to fluctuations in the particle-in-cell method.

Initial conditions: Initially the computational domain contains only subAlfvén and subsonic upstream flow with a homogeneous spatial distribution and a Maxwellian velocity distribution. The magnetic field and electric fields are $\mathbf{B} = \mathbf{B}_0$ and $\mathbf{E} = -\mathbf{U}_0 \times \mathbf{B}_0 / c$. Inside Titan the electromagnetic fields are $\mathbf{E} = 0$ and $\mathbf{B} = \mathbf{B}_0$, and the bulk velocities of ions and electrons also equal to zero.

At $t > 0$ we begin to inject the pickup ions with a spatial distribution according to Eqs. (18) and (21), and a Maxwellian distribution in velocity with the thermal velocity, $v_{th,pi} = 0.25 \text{ km/s}$. Far upstream ($x = -13L$, where $L = R_T$), the ion flux is assumed to have a Maxwellian distribution:

$$f = n_{\infty} (\pi v_{th}^2)^{-3/2} \exp \left[-\frac{(\mathbf{v} - \mathbf{U}_0)^2}{2v_{th}^2} \right], \quad (12)$$

where v_{th} and \mathbf{U} are the thermal and the bulk velocities of the upstream flow, respectively.

Boundary conditions: On the side boundaries ($y = \pm DY/2$ and $z = \pm DZ/2$), periodic boundary conditions were imposed for

incoming flow particles. The pickup ions exit the computational domain when they intersect the surfaces $y = \pm(DY/2 - 5 \times \Delta y)$ or $z = \pm(DZ/2 - 5 \times \Delta z)$ or $x = 14L - 5 \times \Delta x$. Thus there is no influx of pickup ions at the side boundaries. At the side boundaries we also use a damping boundary condition for the electromagnetic field (see, e.g., Lipatov and Combi, 2006; Umeda et al., 2001). This procedure allows us to reduce outgoing electromagnetic perturbations, which may be reflected at the boundaries. At the downstream boundary ($x = 14L$), we use a “Sommerfeld” radiation condition for the magnetic field (see, e.g., Tikhonov and Samarskii, 1963) and a free escape condition for particles with re-entry of a portion of the particles from the outflow plasma. The magnetic field and electric fields are $\mathbf{B} = \mathbf{B}_0$ and $\mathbf{E} = -\mathbf{U}_0 \times \mathbf{B}_0/c$.

Inside Titan, the electromagnetic fields are $\mathbf{E} = 0$ and $\mathbf{B} = \mathbf{B}_0$, and the bulk velocities of ions and electrons are zero. We also take into account the effect of the finite conductivity of Titan's body so that

$$R_{m,eff} = R_{m,up} \quad \text{for } r > r_{exobase},$$

$$R_{m,eff} = R_{m,iono} \quad \text{for } R_T < r \leq r_{exobase},$$

$$R_{m,eff} = R_{m,T} \quad \text{for } r \leq R_T,$$

where $R_{m,up}$, $R_{m,iono}$, and $R_{m,T}$ denote the effective magnetic Reynolds numbers ($R_m = 4\pi U_0 L \sigma_{eff}/c^2$), the values of which were presented in Section 3. The length scale $L = R_T$ is used through the paper. At Titan's surface, $r = R_T$, the particles are absorbed (all runs in Table 1). Due to the absorption distance of $r = R_T$, there are no particles inside Titan. There is no boundary condition for the electromagnetic field, and we also use our equations for the electromagnetic field, Eqs. (13)–(15) and (7) inside Titan but with internal conductivity and the bulk velocity that is calculated from the particles. In this way the jump in the electric field is due to the variation of the value of the conductivity and bulk velocity across Titan's surface. Note that there are no particles inside Titan due to the absorption distance of $r = R_T$. Note that the position of Titan is $x = 0$, $y = 0$, $z = 0$.

The 3D computational domain has dimensions $DY = 30L$, $DZ = 30L$, and $DX = 27L$, where $L = R_T = 2575$ km. We used a mesh of $301 \times 301 \times 276$ grid points, and 4.5×10^8 and 8×10^7 particles for protons and for each species of pickup ions, respectively, for a homogeneous mesh computation. The time step for the particle pushing (Δt_p) satisfies the condition $U_0 \Delta t \leq \min(\Delta x, \Delta y, \Delta z)/16$, whereas time step for electromagnetic equation (Δt_p) satisfies the condition $U_0 \Delta t \leq \min(\Delta x, \Delta y, \Delta z)/(16 \times 64)$.

The global physics in Titan's environment is controlled by a set of dimensionless independent parameters such as M_A , β_i , β_e , M_{pi}/M_p , ion production and charge exchange rates, magnetic Reynolds numbers, and the ion gyroradius $\varepsilon = \rho_{ci}/R_T$. The model of Titan may also be very important in the formation of the inductive magnetosphere. Here $\rho_{ci} = U_0/(eB/M_i c) = M_A c/\omega_{pi}$ and the ion plasma frequency $\omega_{pi} = \sqrt{4\pi n_0 e^2/M_i}$.

For real values of the magnetic field the value of the H_2^+ upstream ion, H_2^+ and CH_4^+ pickup ion gyroradii are about 200–400 km, 200–400 km and 1500–3000 km (respectively) which are calculated from the local bulk velocity. The grid spacing has the value $\Delta x = 257.5$ km.

In order to study ion kinetic effects (e.g., excitation of low-frequency oscillations ($\omega \ll \Omega_b$) by the mass loading), we must satisfy the condition $\Delta \leq (10-20)c/\omega_{pb}$, where Ω_b and ω_{pb} denote the gyrofrequency and the plasma frequency for upstream ions (Winske et al., 1985). The above estimation of the plasma parameters shows that we have good resolution for the low-frequency waves. To excite high-frequency waves ($\Omega_b \ll \omega \ll \Omega_e$) we must satisfy the condition $\Delta \leq 0.25c/\omega_{pb}$ (Winske et al., 1985) for upstream ions. The above estimation shows that we have insufficient resolution for the high-frequency waves.

2.2. Ion–electron collisions

v_{se} and v_{so} are slowing-down collision frequencies between ions and electrons, and ions and neutrals that may include Coulomb collisions. The ion–electron collision frequencies, which are used in Eq. (2), may be estimated as

$$v_{se} = \frac{4\sqrt{\pi}(\ln A)e^4 Z_s^2 n_s}{3\sqrt{M_s} T_s^{3/2}}, \quad (13)$$

where T_s denotes the ion temperature in eV and $\ln A$ is the Coulomb logarithm (see, e.g., Braginskii, 1965, pp. 215–216). For the typical upstream and pickup ion parameters $T_s = (50-300)$ eV (ion temperature) and $n_0 = (0.1-10-1000) \text{ cm}^{-3}$ (density) the collision ion frequency is $v_{se} \approx (0.03-6-600) \times 10^{-8} \text{ s}^{-1}$. Note that a collision time $v_{se}^{-1} \approx (10^6-10^8) \text{ s}$ is much larger than a transition time $t_{transit} = (10^2-10^3) \text{ s}$ in a region above and below the exobase.

The electron–ion collision frequencies, which appear in Eq. (7), may be estimated as

$$v_{es} = \frac{4\sqrt{2\pi}(\ln A)e^4 Z_s n_e}{3\sqrt{m_e} T_e^{3/2}}, \quad (14)$$

where T_e denotes the electron temperature in eV and $\ln A$ is the Coulomb logarithm (see, e.g., Braginskii, 1965, pp. 215–216). For the typical electron parameters $T_e = (50-200)$ eV and $n_e = (0.1-10.0-1000.0) \text{ cm}^{-3}$ the collision electron–ion frequency is $v_{es} \approx 5 \times (0.1-10.0-1000) \times 10^{-6} \text{ s}^{-1}$. The electron–ion collisions become unimportant in the region above the exobase and important well below the exobase.

2.3. Charged particle–neutral collisions

Charged particle–neutral collision frequencies are calculated depending on the species in question. For plasma, the thermal velocity v'_s (s denotes the ion species) is assumed to be greater

Table 1

The values of the density for the upstream ions, ionospheric ions and the magnetic Reynolds number in the exosphere. The maximum values of the density of atmosphere for different species at the exobase (estimated in Yelle et al., 2006).

Case	$n_{up,H^+} \text{ (cm}^{-3}\text{)}$	$n_{iono,R_{iono},28} \text{ (cm}^{-3}\text{)}$	$n_{atmos,H} \text{ (10}^4 \text{ cm}^{-3}\text{)}$	$n_{atmos,H_2} \text{ (10}^5 \text{ cm}^{-3}\text{)}$	$n_{atmos,CH_4} \text{ (10}^6 \text{ cm}^{-3}\text{)}$	$n_{atmos,N_2} \text{ (10}^7 \text{ cm}^{-3}\text{)}$	$R_{m,exo}$
<i>Model A with magnetospheric H^+ ions in upstream</i>							
a1	0.1	6.25	2.0	8.0	1.2	1.2	2.0
a2	0.1	6.25	2.0	8.0	1.2	1.2	20.0
a3	0.1	6.25	2.0	8.0	1.2	1.2	2.0
<i>Model B with pickup H^+ ions in upstream</i>							
b1	0.02	6.25	2.0	2.0	1.2	1.2	2.0
b2	0.02	6.25	2.0	2.0	1.2	1.2	20.0
b3	0.02	6.25	2.0	2.0	1.2	1.2	2.0

than the drift velocity, so we take

$$v_{s,0} = n_0 \sigma^{0,s} v'_s, \quad (15)$$

where the cross section $\sigma^{0,s}$ is typically about $5 \times 10^{-15} \text{ cm}^2$ and (see, e.g., Mankofsky et al., 1987, Eq. (17)). For the typical pickup and ionospheric ion parameters below exobase $n_0 = (10^7 - 10^{10}) \text{ cm}^{-3}$ (density, see, e.g., Modolo and Chanteur, 2008, Figure 1) and $v_s = 1 \text{ km/s}$ (velocity) Eq. (15) gives the collision ion frequency is $v_{s,0} \approx 5 \times (10^{-3} - 1) \text{ s}^{-1}$. Note that a wide range of collision times $v_{s,0}^{-1} = (0.2 - 10) \text{ s}$ may include a transition time $t_{\text{transit}} = (10^2 - 10^3) \text{ s}$ in a region below the exobase. So that the collisions between ions and neutrals become very important below the exosphere, Eq. (2).

Evaluation of the electron–neutral collisions gives the following expression:

$$v_{e,0} = \sigma^{e,0} n_0 v'_e. \quad (16)$$

In case of N_2 Spencer et al. (2008) suggests the following value of cross section $\sigma^{e\text{N}_2} = 2.33 \times 10^{-11}$. So one may expect a strong electron–neutral collision effects only well below the exobase. In our modeling we assume that $|\mathbf{U}_i - \mathbf{U}_s| \ll J/(ne)$ and we drop the third and fifth terms from the right side of Eq. (7). Finally, the generalized Ohm's law looks like the following:

$$\mathbf{E} = \frac{1}{en_e c} (\mathbf{J} \times \mathbf{B}) - \frac{1}{en_e} \nabla p_e + \frac{m_e}{e} \sum_s v_{e,s} \frac{\mathbf{J}}{ne}. \quad (17)$$

2.4. Ionization processes

Electron impact: The impacting ions consist both of upstream torus ions as well as newly implanted ions which are picked up by the motional electric field. Electron impact ionization production rates are calculated with the following expressions:

$$q_{s,\text{impact}1} = v_{s,1} n_{e,\text{up}} n_{\text{neutral},s},$$

$$q_{s,\text{impact}2} = v_{s,2} n_{e,\text{pi}} n_{\text{neutral},s}, \quad (18)$$

where $n_{e,\text{up}}$ is the magnetospheric electron density, $n_{e,\text{pi}}$ is the density of electrons connected with the pickup ions, $n_{\text{neutral},s}$ is the neutral density of the species s (Eq. (9)), $v_{s,1}$ is ionization rate by electron impact (Table 2). The electron impact rates were chosen from Sittler et al. (2005). Since the rates depend on the energy of the particles, we use a range of the values of these parameters to study how the numerical solution depends on these parameters. Electron impact was used for creating H^+ , H_2^+ , N_2^+ and CH_4^+ ions. The generation of ions due to electron impact was produced with a variable weight of the macro-particles (see, e.g., Lipatov, submitted for publication).

Photoionization production: We use the algorithm for photo-production by Simon et al. (2006). The decrease dl of solar UV intensity due to absorption processes can be obtained from

$$\frac{dl}{l} = \sum_s \sigma_{v,s} n_{\text{neutral},s}(r) \frac{dr}{\cos \chi_v}, \quad (19)$$

where $\sigma_{v,s}$ denotes the absorption cross-section for the species s and χ_v is the solar zenith angle. Integration of Eq. (19) yields

$$l(r) = l_\infty \exp \left[-\frac{1}{\cos \chi_v} \int_r^{r_{\text{max}}} \sum_s \sigma_{v,s} n_{\text{neutral},s}(\xi) d\xi \right], \quad (20)$$

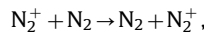
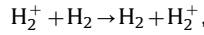
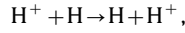
where l_∞ and r_{max} denote the solar wind flux at the top of the atmosphere and the maximum radius of an extension of neutral components. In our model $r_{\text{max}} = 8R_T$. However, in Titan's environment the value $r_{\text{max}} = 3R_T$ is also a good approximation (see, e.g., Simon et al., 2006). The integral on the right side was estimated numerically in form of array $\Psi = \Psi(r)$ for the use in our global modeling.

Finally, the ion production function q_v is given by

$$q_{v,s}(r) = v_s n_{\text{neutral},s}(r) \exp \left[-\frac{\sigma_{v,s}}{\cos \chi_v} \Psi(r) \right], \quad (21)$$

where $v_s = \sigma_{v,s} l_\infty$ denotes the photoionization frequency.

Charge exchange: The interaction of ions with neutral particles by charge exchange (see Lipatov and Combi, 2006, Eqs. (12)–(15)) currently included for the following reactions:



A more complete list of reaction (see, e.g., Sittler et al., 2005, Table 3c) will be considered in future modeling. It needs of course the addition of Monte Carlo computations. However, this approach is beyond the scope of this paper.

Our code solves Eqs. (2)–(6), (16)–(22).

2.5. Numerical method

We employed a standard particle-in-cell (PIC) method with a homogeneous grid. The time integration of the particle equations of motion uses a leapfrog scheme. The time integration of the electromagnetic field equations uses an implicit finite difference scheme (see, e.g., Lipatov, 2002). We used different time steps for particle (Δt_p) and field (Δt_f) pushing (subcycling), where $\Delta t_p = \min(\Delta x, \Delta y, \Delta z)/(16U_0)$ and $\Delta t_f = \min(\Delta x, \Delta y, \Delta z)/(64U_0)$. The code was optimized for massively parallel computation: (a) using the open multi-processing (OpenMP) and (b) using the hybrid environment—message passing interface (MPI) along the computational nodes and the open multi-processing (OpenMP) inside the node.

Since the gyroradius must be resolved, a grid point spacing of less than 1 gyroradius is required in order to avoid scheme dispersion and dissipation. On the other hand, good statistics are required, therefore a sufficiently large number of particles per cell have to be used (i.e., to obtain low “shot” noise, which manifests itself as fluctuations in the plasma parameters due to a small number of particles per cell).

Table 2

Photoionization rates, electron impact ionization rates (for pickup and upstream electrons) and charge exchange cross sections. From Sittler et al. (2005). In modeling: $l=0.25$ (cases a1, a2, b1, and b2) and $l=1$ (cases a3 and b3).

Species	$v_{ph} (10^{-9} \text{ s}^{-1})$	$\sigma_v (10^{-18} \text{ cm}^2)$	$v_{eim,pi} (10^{-9} \text{ cm}^3 \text{ s}^{-1})$	$v_{eim,up} (10^{-8} \text{ cm}^3 \text{ s}^{-1})$	$\sigma_{cex} (10^{-16} \text{ cm}^2)$
H^+	1.8	3.8	$(0.3-1) \times 5.13$	$l \times 3.1$	22
H_2^+	0.59	1.3	$(0.3-1) \times 6.3$	$l \times 5.13$	2.9
CH_4^+	6.5	14	$(0.5-1) \times 2.33$	22.0	0.57
N_2^+	3.9	8.4	$(0.5-1) \times 1.02$	16.4	3

3. Results of the modeling

To study the interaction of the magnetospheric plasma with the ionosphere of Titan the following sets of the magnetospheric plasma and ionosphere parameters were adopted in accordance with flyby observational data: upstream velocity, $U_0=257.5$ km/s; $\mathbf{U}_0/U_0 = (0.97, -0.2, 0.136)$; $W_0=34.9$ km/s; magnetic field, $B_0=5.59$ nT; $\mathbf{B}/B_0 = (0.46, 0.82, -0.34)$. The upstream velocity components are based on Cassini plasma spectrometer observations (Sittler et al., 2010, Figure 8). The other upstream parameters are used for model A: density and temperature, $n_0 = n_{H^+} = 0.1$ cm $^{-3}$ and $T_p=201$ eV, Alfvén Mach number and proton beta, $M_A=0.75$; $M_s=0.67$; $\beta_{H^+} = 0.35$. Note here that we used the various magnetic Reynolds number for cases (a1), (a2) and (a3) (see the last column from Table 1).

The other upstream parameters are used for model B: density and temperature, $n_0 = n_{H^+} = 0.02$ cm $^{-3}$; $T_p=441$ eV, Alfvén Mach number and proton beta, $M_A=0.44$; $M_s=0.41$; $\beta_{H^+} = 1.13$. The values of the electron betas are $\beta_{e,0} = 1$ ($T_e=200$ eV); $\beta_{e,2} = 0.025-0.25$ ($T_{pickup,e}=5-50$ eV). Note here that we used the various magnetic Reynolds number for cases (b1), (b2) and (b3) (see the last column in Table 1).

Atmospheric density for the considered species, the photoionization rates, electron impact ionization rates and charge exchange rates are presented in Tables 1 and 2.

A realistic magnetic Reynolds number in the upstream plasma is about 5×10^8 , and its value may be lower by factor $10^{-6}-10^{-7}$ (see Section 3.4) inside the ionosphere. However, in our modeling we have chosen a much lower effective magnetic Reynolds number to suppress a “shot” noise. The effective magnetic Reynolds numbers of the upstream and ionospheric plasmas are $R_{m,up} = 200$, $R_{m,iono} = 2-200$, whereas for Titan’s body the magnetic Reynolds number is $R_{m,T} = 0.2-2$. We use the following values of the particle and electromagnetic field time steps: $\Delta t_p = 0.07$ s and $\Delta t_f = 0.001$ s.

Since many plasma and atmospheric parameters are still uncertain, we have studied two basic models with a wide range of parameters such the electron impact ionization production rates (Table 2) and H_2 neutral production rates (Table 1) in order to choose the best ones for interpretation of the observational data. We present here a sample of the wide range of modeling results, which we have explored and which were in varying degrees of agreement or disagreement with observations in order to illustrate the dependence of the plasma environment near Titan on various values input parameters. We also explored the physical response of the global system to various parameter values and regimes. Tables 3 and 4 present the total production rates and escape flux for pickup ion.

3.1. Global structure of Titan’s environment (T9 encounter)

In this section we discuss the results of modeling at time $t = 11T_{transit} \approx 3400$ s, where $T_{transit}$ denotes an average transition

Table 3
Total production rate for pickup ions.

Case	$G(H^+) 10^{26} s^{-1}$	$G(H_2^+) 10^{26} s^{-1}$	$G(CH_4^+) 10^{26} s^{-1}$	$G(N_2^+) 10^{26} s^{-1}$
<i>Model A with magnetospheric H^+ ions in upstream</i>				
a1	1.66	34.6	5.62	37.0
a2	3.2	72.4	7.34	43.2
a3	6.48	235.4	6.48	43.2
<i>Model B with low density H^+ ions in upstream</i>				
b1	6.5	19.0	16.8	43.2
b2	12.1	38.0	21.3	120.7
b3	15.5	77.7	19.44	118.8

Table 4
Pickup ion escape flux.

Case	$G(H^+) 10^{25} s^{-1}$	$G(H_2^+) 10^{25} s^{-1}$	$G(CH_4^+) 10^{25} s^{-1}$	$G(N_2^+) 10^{25} s^{-1}$
<i>Model A with magnetospheric H^+ ions in upstream</i>				
a1	0.18	7.7	0.8	4.5
a2	0.25	10	1.3	8
a3	0.38	12.4	0.4	1.5
<i>Model B with low density H^+ ions in upstream</i>				
b1	0.06	0.52	0.24	1.3
b2	0.09	0.7	0.42	2.6
b3	0.06	0.64	0.24	1.6

time for an upstream particle to travel from the left (upstream) boundary to the right (downstream) boundary.

Let us consider first the global picture of the interaction of Saturn’s plasma with Titan when $\rho_{H^+} = 0.1$ cm $^{-3}$ (model A) and $\rho_{H^+} = 0.02$ cm $^{-3}$ (model B).

Fig. 2(a), (b) demonstrates the asymmetrical wing-like distribution of pickup ions H^+ with densities for model A (a) and model B (b) in the y - x (left), y - z (middle) and z - x (right) planes. Pickup ion motion is determined mainly by electromagnetic drift. The motion along the magnetic field is due to the thermal velocity and the gradient of the electron pressure. In model B the density profile is extended in the x -direction, Fig. 2(b). At the side boundaries pickup ions escape the computational domain.

Fig. 2(c), (d) shows the distribution of the pickup ion’s H_2^+ density. The H_2^+ ion density profiles are similar to the H^+ ion density profiles, but the H_2^+ ion density is higher by factor of 10 in comparison with H^+ distribution. The H^+ and H_2^+ pickup ions are created mostly by photoionization and electron impact ionization.

The heavy N_2^+ and CH_4^+ pickup ions are already “unfrozen” due to their large gyroradii and they penetrate through H^+ and H_2^+ ions at distances of gyroradii across the magnetic field. Fig. 3(a), (b) shows the density distribution of N_2^+ heavy pickup ions in the y - x , y - z and z - x planes. One can see the formation of the Alfvén wing oblique to the y -axis. Note that these Alfvén wings have the same location as the Alfvén wing for the maximum density of H^+ and H_2^+ pickup ions (compare with Fig. 2). At the front of the Alfvén wing one may see a strong gradient in the density of pickup ions. The velocity distributions of the heavy pickup ions are the ring or shell-like distributions. Such type of distribution may cause generation of an ion cyclotron waves in the plasma wake (see, e.g., Cowee et al., 2010) and details of these distributions were discussed in Lipatov et al. (2011). Here we do not show the distribution of the CH_4^+ heavy ions because their distribution is similar to the N_2^+ ion distribution. The plasma wake demonstrates a formation of time-dependent structuring in the pickup ion tails, accompanied by a splitting of the heavy pickup ion tails due to a strong polarization electric field. Such finite gyroradius effects were also observed in 2.5 D hybrid and bi-fluid modeling of a weak comet (see, e.g., Lipatov et al., 1997; Sauer et al., 1996, 1997; Lipatov, 2002). Remember that the orientation of the pickup ion tail depends strongly on the gas production/ionization rate.

Fig. 3(c), (d) shows the upstream H^+ ion density profile in the y - x , y - z and z - x planes. One may see density depletion inside the Alfvén wing. The asymmetrical distribution of the incoming ions in the y - z plane may be explained by the existence of the B_z component of the upstream magnetic field. The inclination of the magnetic field results in an asymmetrical boundary condition for ion dynamics (penetration and reflection) in Titan’s ionosphere and an asymmetrical Alfvén wing. The density profile is a little bit disturbed near the side boundaries. However, as already discussed, this perturbation does not affect the region close to Titan.

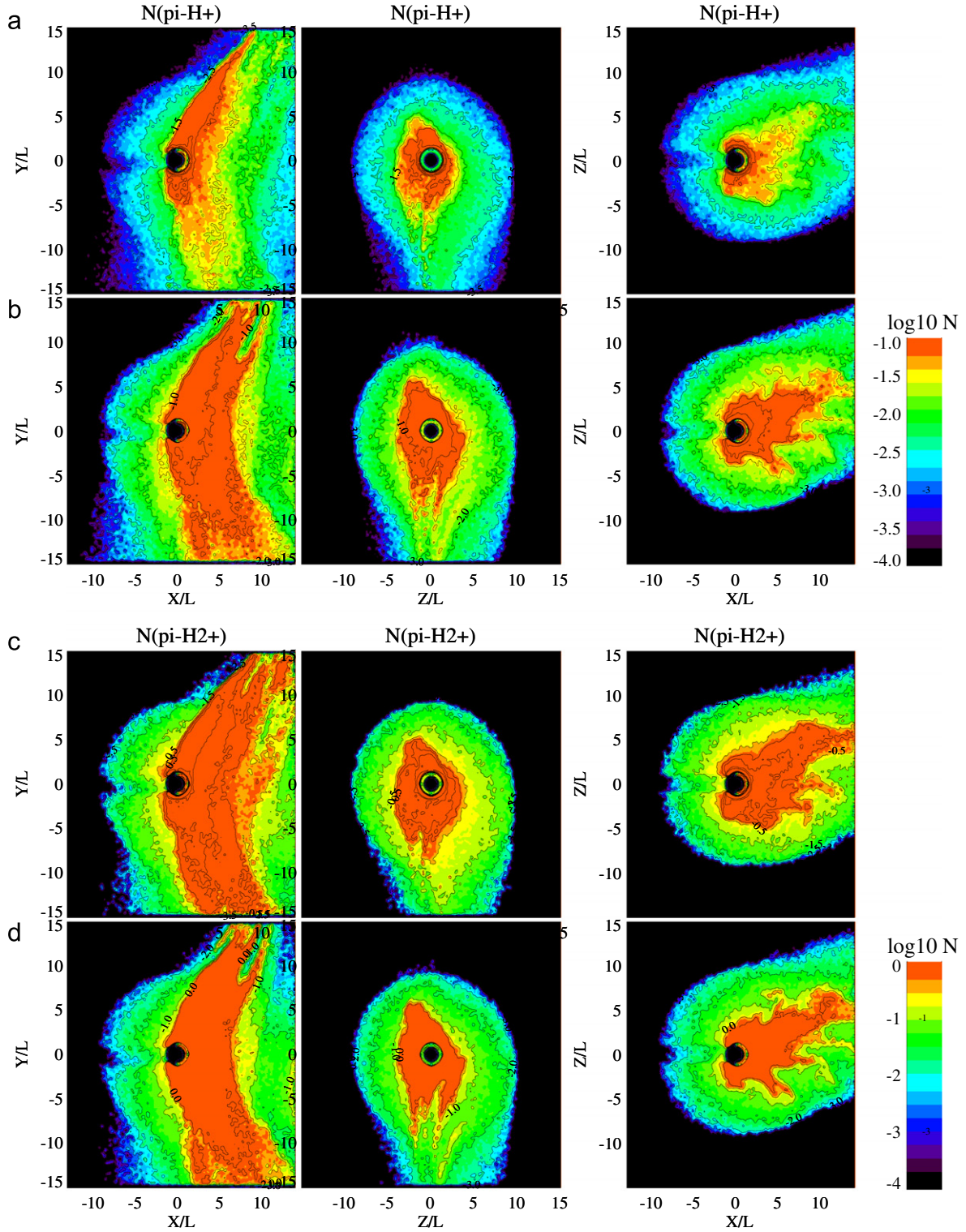


Fig. 2. The 2D cuts of the pickup ion H^+ and H_2^+ density profile ($\log_{10}(n/n_0)$): model A (a, c), model B (b, d).

Fig. 4 shows the density distributions for the ionospheric ions. One can see the shell-like distributions. Note that the ionospheric ions move mainly in the radial direction with a weak expansion in the angular directions. Since we assume that ion production is mostly due to photoionization we did not create ionospheric ions in the region with $x < 0$.

Mass loading of the upstream flow with light (H^+ , H_2^+) and heavy (N_2^+ , CH_4^+) pickup ions results in the excitation of the low

frequency waves since the velocity distribution of the pickup ions already have the ring or shell-like distribution. Such types of distributions are unstable and may generate kinetic Alfvén waves, ion cyclotron waves and whistler waves. The 3D hybrid modeling demonstrates complicated wave structures because of the presence of the multi-mass ion species that excite waves on multi-space/time scales. Note here that finite ion gyroradii also play a very important role in wave excitation.

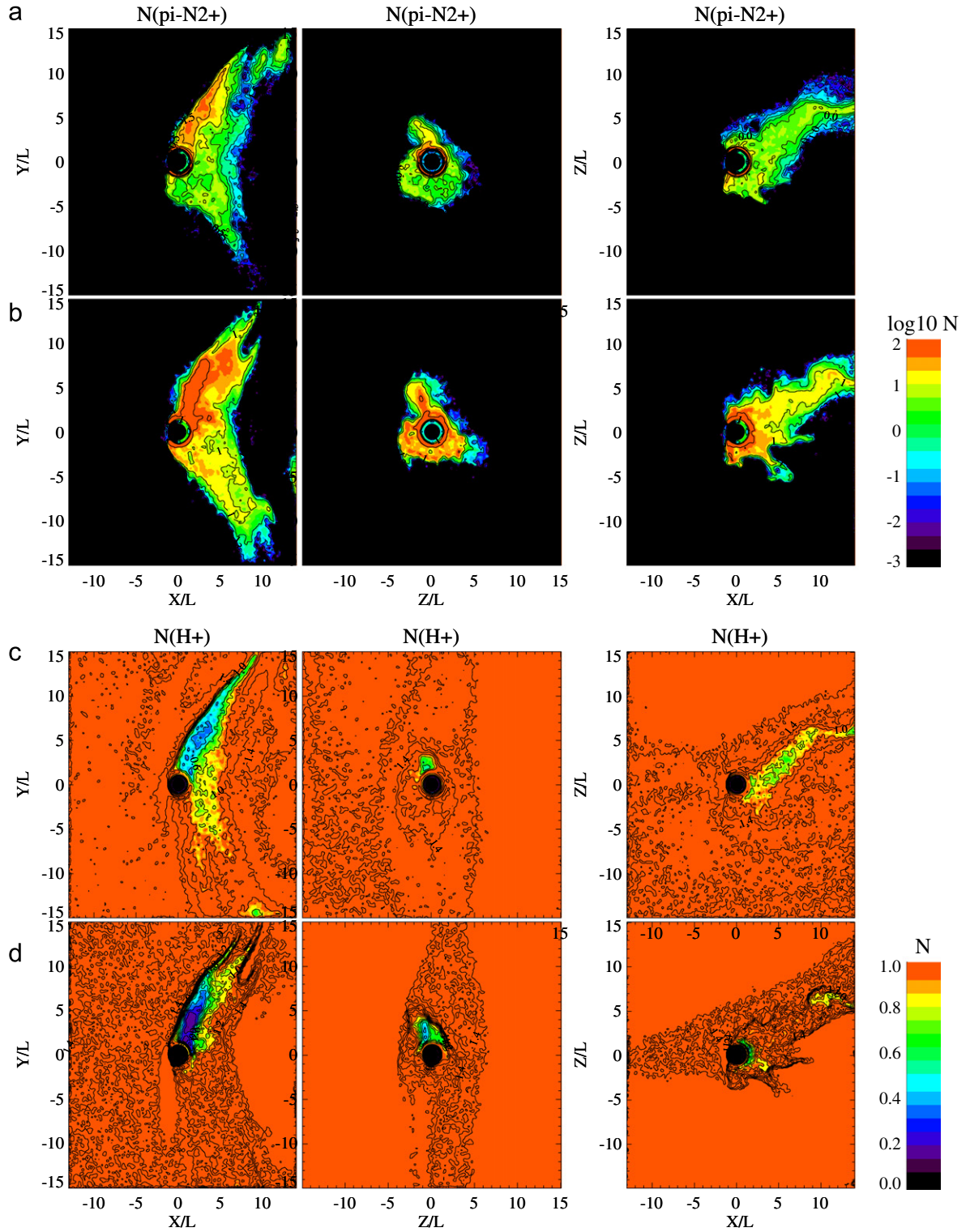


Fig. 3. The 2D cuts of the pickup ion N_2^+ density profile ($\log_{10}(n/n_0)$): model A (a), model B (b). The 2D cuts of the upstream H^+ ion density profile: model A (c), model B (d).

Fig. 5 shows the distribution of the magnetic field component B_z in the y - x , y - z and z - x planes. One may see the formation of the Alfvén wing in the direction of the incoming magnetic field (top and bottom of the middle figure). Note that both the initial value of the magnetic field ($B=B_0$) and the effective magnetic Reynolds number below the exobase and inside Titan may play an important role in the formation of an inductive magnetosphere near the surface of

Titan. Weak perturbations of the magnetic field ($\omega \approx \Omega_{H_2^+}$) were observed near the ionosphere of Titan. Unfortunately, the nature of these perturbations (“shot” noise or electromagnetic instability) is still unclear. To resolve this question, we still have to produce a model with a much larger number of macro-particles and with much better spatial resolution below the exobase. The results of this study will be discussed in a future publication.

3.2. Comparison with CAPS and magnetic field observational data

The results of the measurements by the particles and field instruments on the Cassini spacecraft during the T9 encounter provided new and important information with which realistic modeling for the plasma interaction can be tested. Along that

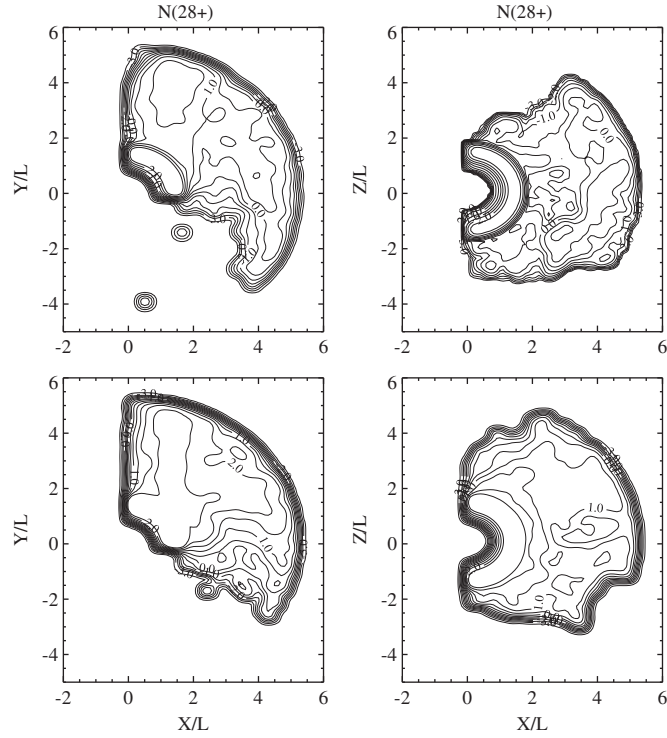


Fig. 4. The 2D cuts of the ionospheric $M=28$ ion density profile ($\log_{10}(n/n_0)$): model A (top), model B (bottom).

trajectory physical signatures of the wake were seen as one sharp strong peak (event 1) and a broad weak peak (event 2) in the total ion density profile (without upstream ions). The locations of event 1 and event 2 inside the trajectory are 18:20UT–18:43 ($Y=0-3R_T$) and 19:07UT–19:30UT ($Y=0-6.5R_T$).

In order to fit the observational data we performed modeling for model A (high density of H^+ ions in upstream flow) and model B (very low density of H^+ ions in upstream flow) for various total ion production rates for the ionospheric ions ($M=28$ amu) and H_2^+ pickup ions, see Table 1. This approach allows us to find the best case of the computational model that may fit the observational data. In model A (cases a1, a2, and a3) the production rate for H_2^+ pickup ions is four times higher than the standard value used in other cases. In model B (cases b1, b2, and b3) the production rate for ($M=28$ amu) ionospheric ions is four times higher than a standard value used in model A (cases a1, a2, and a3) to better fit the observational total ion density.

Fig. 6 shows the total ion density (without upstream ions) along the Cassini trajectory from the CAPS measurements (\bullet) (Sittler et al., 2009, 2010). The densities of the pickup ions and upstream ions produced in the 3D hybrid model are the following: the total pickup ions density— $N_{pi,tot}$ (solid line), the light pickup ion density— H^+ (Δ) and H_2^+ ($*$), the heavy pickup ion densities— N_2^+ density (\diamond) and CH_4^+ (\times), the active ionospheric ion density— $M=28$ amu ($+$), and the upstream ion density (squares). Here, $Y(R_T)$ denotes the same notation as it was used in Modolo et al. (2007b), namely, $Y(R_T)$ is a projection of the spacecraft trajectory onto the y -axis.

Let us consider first the results of the modeling with model A (left column). In case a1 (Table 1) the maximum value exceeds the density observed by a factor of 3 in event 1, Fig. 6 (left, top). The main input in the peak value is due to N_2^+ , CH_4^+ and N_2 pickup ions. In event 2 the value of the model's density exceeds the observation data but is only in qualitative agreement with observation. The total ion density profile agrees well with that derived from the upper hybrid resonance frequency combined

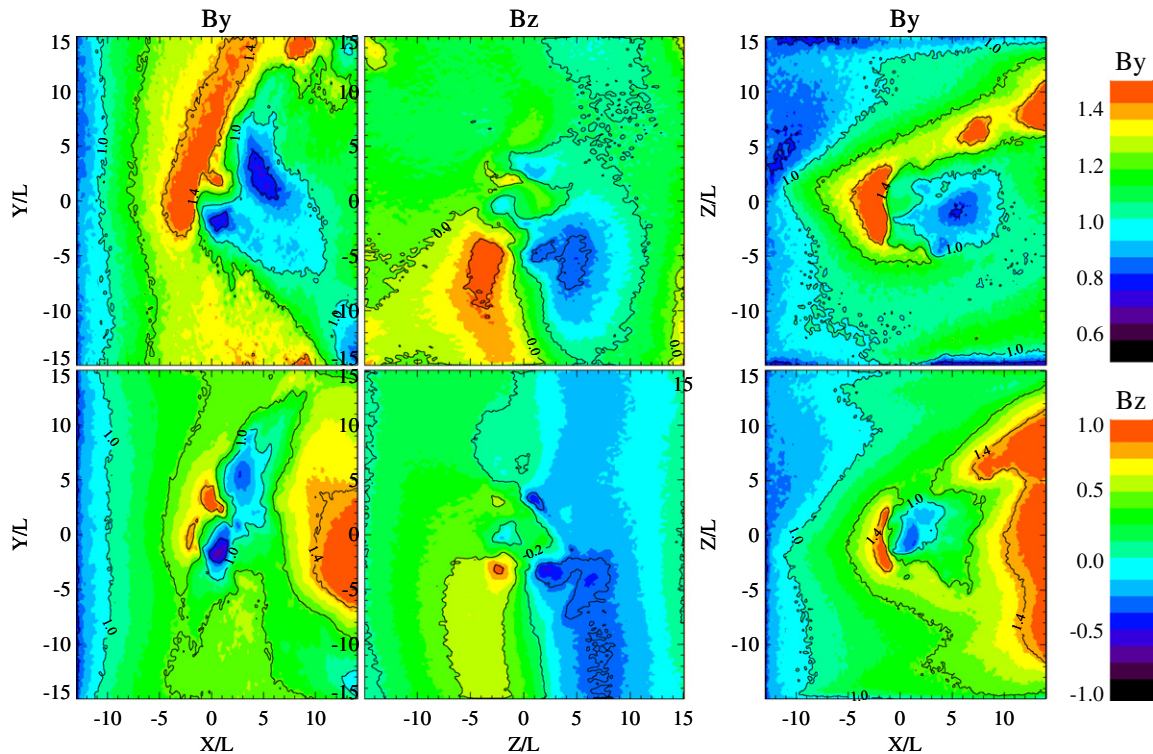


Fig. 5. The 2D cuts of the magnetic field B_y (B/B_0) and B_z (B/B_0) profiles: model A (top), model B (bottom).

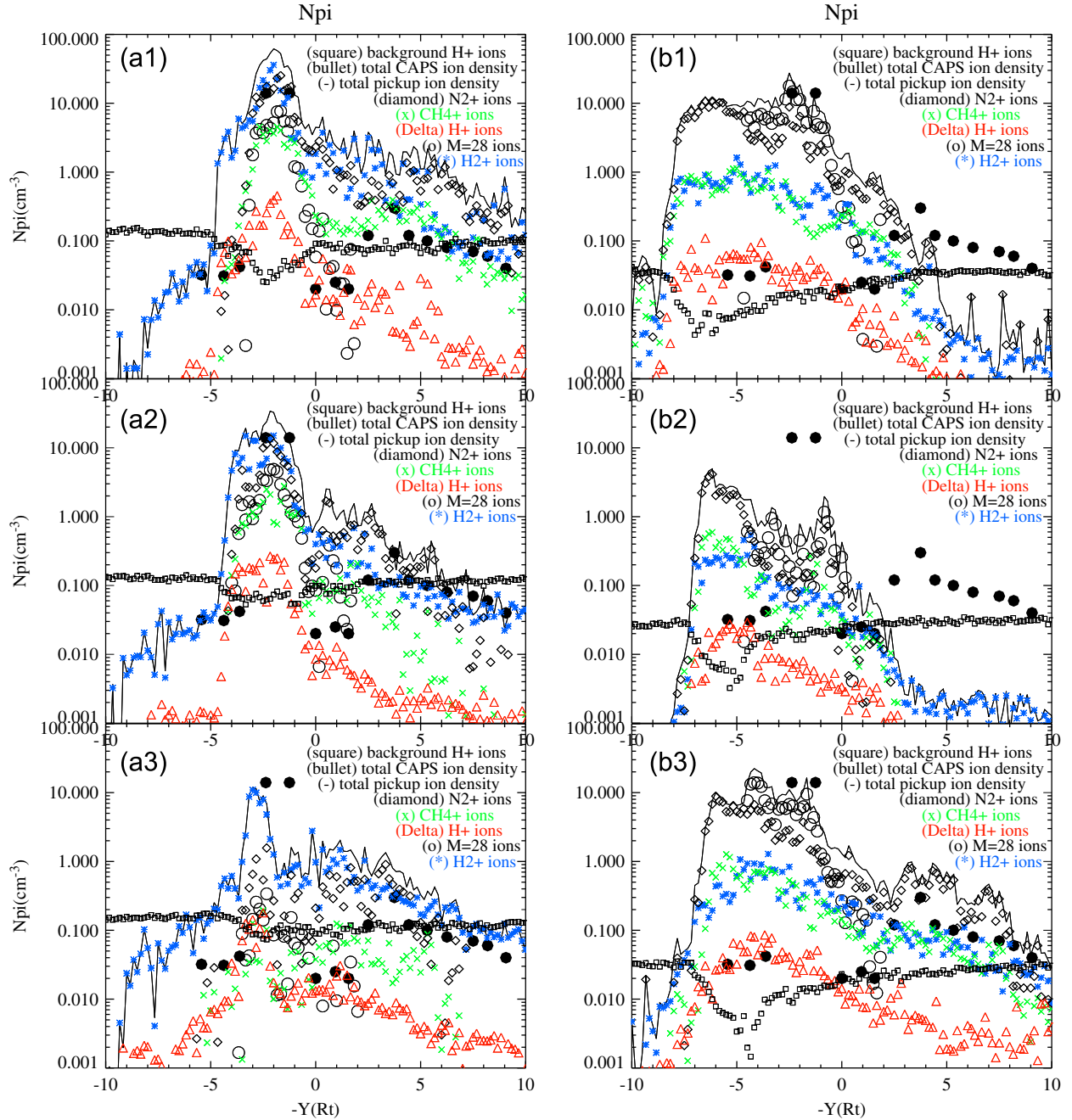


Fig. 6. Ion densities along the Cassini trajectory (cm^{-3}).

with Langmuir probe observations from Modolo et al. (2007b). The total ion density produced in the hybrid modeling of Modolo et al. (2007a) also shows good agreement with the RPWS experiment. However, the inbound and outbound values of the total density in their model are higher by factor of 5–10 than observed values in the RPWS experiment. The main peak of the total ion density in the modeling of Modolo et al. (2007a) is smaller by a factor of 2.5 than the observed value. These differences in the total ion density may be explained by an inclusion of heavy O^+ ions in the upstream plasma in their model.

In cases a2 and a3 the modeling matches the density profile in event 1 and event 2 much better, Fig. 6 (left column—middle and bottom). In case a2 the peak of the pickup ion total density is very close to observation in event 1 ($1R_T < y < 3R_T$). In event 2, the pickup ion density profile is in good agreement with observation

($-4R_T < y < -10R_T$) except for the lack of depletion in the pick up ion density at $y = -1R_T$. In case a3 the modeling shows a much better agreement with an observation in event 1 but it produces a little bit higher pickup ion density in event 2, Fig. 6.

Let us consider now the results of the modeling with model B (right column). In cases b1, b2 and b3, the model gives a wider peak in the event 1 than in all cases for model A. In event 2 cases b1 and b2 produce a much lower pickup ion density than it was observed. In case b3 the modeling produces a higher pickup ion density in event 2, Fig. 6. Note that the composition of the peak of the density in event 1 for model A is determined mostly by H_2^+ , the heavy pickup ions and the ionospheric ions, whereas for model B it is determined mostly by N_2^+ pickup and ionospheric ions. The composition of the peak in the pickup density in event 2 for model A is determined mostly by H_2^+ and N_2^+ pickup ions,

whereas for the model B it is determined mostly by H^+ and H_2^+ pickup ions.

We should also note that the hybrid modeling for T9 with heavy ions upstream (see, e.g., Simon et al., 2007a, 2007b) produces another picture of the plasma-Titan interaction because of a deeper penetration of these ions into the ionosphere. The heavy ions from the upstream flow transfer the motional electric field into the exosphere. Thus, pickup ions can gain a larger energy than is possible without heavy ions in the upstream flow. The MHD and Hall-MHD modeling with light and heavy ions upstream produces only one smooth peak in the plasma density profile between event 1 and event 2 (Ma et al., 2007). The maximum values of the electron density profile are about 2 cm^{-3} and 3 cm^{-3} for the MHD and Hall-MHD models, respectively. Recall that the CAPS observations give the total pickup ion density about of 10 cm^{-3} . However, the CAPS measurements did not confirm the existence of the heavy ions upstream.

Let us now compare the magnetic field from our model with observation. Fig. 7 shows the magnetic field profiles along the Cassini trajectory. The magnetic field profiles B_x and B_y do not match the observational data very well for either model A or B. Our model does not produce the observed strong variations in B_x in the region near $y = -5R_T$, Fig. 7 (top). The magnetic field profile B_z matches the observational data quite well with variations about of 0.5 nT. Future modeling must use much better spatial grid resolution below the exobase. We must also use a realistic inhomogeneous Saturn magnetic field for the boundary conditions and, possibly, inhomogeneous upstream flow parameters. Our analysis of all the models run (many more than presented in this paper) finds that these two cases (A and B) show a reasonably good fit to the observational data. The hybrid modeling performed by Simon et al. (2007a, 2007b) produces a good agreement with the magnetic field observations, however, their modeling includes a heavy species of mass $M_i = 14$ amu that may change the physics of the interaction between Titan and Kronian magnetosphere. The hybrid modeling performed by Kallio et al. (2007) also produces a good agreement with the observed magnetic field but only in a case with the O^+ ions in the upstream flow. In the case with no O^+ ions in the upstream flow, their modeling does not produce

any agreement with observed magnetic field. The very important point in our modeling is that we use a homogeneous magnetic field as the upstream (Saturn's magnetosphere) magnetic field. In future modeling, we must take into account a more realistic magnetic field.

4. Conclusions

A 3D hybrid (Boltzmann) modeling of Titan's plasma environment during the T9 encounter involving six ion species demonstrated several new features:

- Modeling with high-density magnetospheric H^+ ions and with low density upstream pickup ions with high beta (β_{H^+}) produces approximately similar results.
- Heavy pickup ions form a structured wake.
- Magnetic field barrier formation and Alfvén wing formation.
- The electron temperature plays an important role in plasma structure formation, and in creating the ion fluxes inside the ionosphere.
- Modeling demonstrates a quantitative agreement between the densities of the upstream and pickup ions observed by CAPS during the T9 encounter. The model with magnetospheric H^+ ions produces a narrow peak in the profile of the heavy pickup ion density distribution (event 1) and a broad profile in the N_2^+ , H_2^+ density distributions (event 2). The ionospheric ions also produce a strong peak in the density profile near the event 1. In our modeling, the peak in the pickup ion's density (event 1) is slightly shifted to the left relative to the CAPS observation. This problem may be related to the correct determination of the bulk velocity upstream.

Our model produces a satisfactory agreement with observation of the total pickup ion (event 1) and upstream ion density. For event 2, the modeling produces a higher peak in the density profile. The modeling did not produce yet a strong gap between the peaks in the density profile for event 1 and event 2. The model B produces a wider density profile than it was observed.

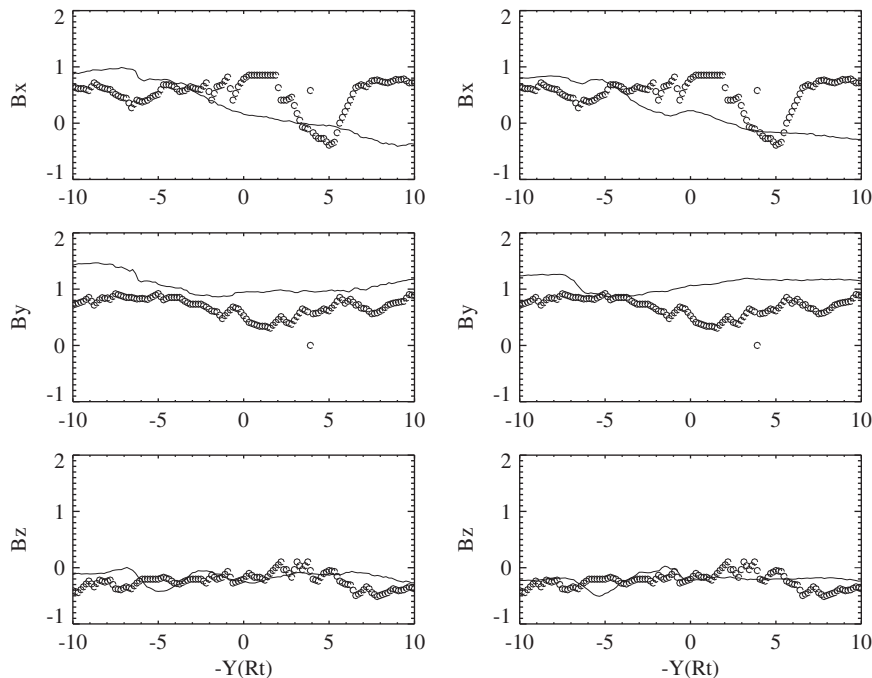


Fig. 7. Magnetic field (B/B_0) for T9 encounter. \circ —Cassini observation (Bertucci et al., 2007); solid line—modeling: model A (left), model B (right).

The improved model will need a much better spatial resolution and a detailed description of the chemical and collision processes below the exobase. The essential part of our modeling is the absence of heavy ions in the upstream flow in accordance with the CAPS measurements. The hybrid modeling for the T9 with heavy ions upstream (see, e.g., Simon et al., 2007a, 2007b; Modolo et al., 2007a) produces another picture of plasma-Titan interaction because of a deeper penetration of heavy upstream ions into the ionosphere. The MHD and Hall-MHD models, which also include the heavy ions in the upstream flow, produce only one wide peak in the density profile between events 1 and 2 (Ma et al., 2007). The comparison between energy and momentum distributions for pickup ions in modeling and in observations needs details of the velocity distribution dynamics. Such comparisons have been discussed in Lipatov et al. (2011).

Modeling demonstrates a satisfactory agreement only with observations of the B_z magnetic field component. Further improvement is needed in our computational model for better agreement in the B_x and B_y magnetic field components. To do that we have to take into account the inhomogeneous magnetospheric magnetic field. The interpretation of the processes in Titan's plasma environment for the T9 encounter is much more complicated than for the TA encounter since the trajectory of the T9 encounter is very close to the Alfvén wing. In this encounter the spacecraft has moved near the Alfvén wing, where a strong electromagnetic oscillation may occur. Thus, it would be difficult to discover upstream parameters from the CAP observations.

Our further modeling will address to much accurate spatial resolution of wave-particle interactions. The future modeling will use the composite grid structure, e.g., “Cubed sphere”, “Yin-Yang” grids (see, e.g., Koldoba et al., 2002; Kageyama and Sato, 2004; and references therein) incorporated into the Cartesian grid to resolve the multiscale and collision dominated effects near the surface of Titan and the outer plasma environment. It will allow us to resolve strong gradients in atmospheric density profile and also the collision processes on the small scale in the region below the exobase. A full hybrid modeling for the plasma including an electron temperature treatment that accounts for electron-neutral collisions and a detailed neutral description would be required to produce an accurate global picture from first principles.

Acknowledgments

A.S.L., E.C.S., R.E.H., J.F.C., and D.G.S. were supported by the Grant Analysis of Titan's Interaction with Saturn's Magnetosphere using Cassini Titan Flyby Data and Kinetic-Fluid Model from the NASA Cassini Data Analysis Program (08-CDAP08-0043). A.S.L. was also supported in part by the Grants/Tasks 900-37-172 and 670-90-315 between the GPII/(GEST Center) UMBC and NASA GSFC. Computational resources were provided by the NASA Ames Advanced Supercomputing (NAS) Division (Projects SMD-09-1124 and SMD-10-1517). The authors thank the referees for fruitful comments.

References

- Amsif, A., Dandouras, J., Roelof, E.C., 1997. Modeling the production and imaging of energetic neutral atoms from Titan's exosphere. *Journal of Geophysical Research* 102 (A10), 22169–22181.
- Braginskii, S.L., 1965. Transport processes in a plasma. In: Leontovich, M.A. (Ed.), *Reviews of Plasma Physics*, Consultants Bureau, New York, pp. 205–240.
- Brecht, S.H., Luhmann, J.G., Larson, D.J., 2000. Simulation of the Saturnian magnetospheric interaction with Titan. *Journal of Geophysical Research* 105 (A6), 13119–13130.
- Cowee, M.M., Gary, S.P., Wei, H.Y., Tokar, R.L., Russell, C.T., 2010. An explanation for the lack of ion cyclotron wave generation by pickup ions at Titan: 1-D hybrid simulation results. *Journal of Geophysical Research* 115, A10224. doi:10.1029/2010JA015769.
- Cravens, T.E., Lindgren, C.J., Ledvina, S.A., 1998. A two-dimensional multifluid MHD model of Titan's plasma environment. *Planetary and Space Science* 46 (9/10), 1193–1205.
- Hartle, R.E., Sittler, E.C., Neubauer, F.M., et al., 2006. Initial interpretation of Titan plasma interaction as observed by the Cassini plasma spectrometer: comparisons with Voyager 1. *Planetary and Space Science* 54, 1211–1224.
- Kageyama, A., Sato, T., 2004. “Yin-Yang grid”: an overset grid in spherical geometry. *Geochemistry, Geophysics and Geosystems* 5 (9), Q09005. doi:10.1029/2004GC000734.
- Kabin, K., Gombosi, T., De Zeeuw, D., Powell, K., Israelevich, P., 1999. Interaction of the Saturnian magnetosphere with Titan: results of a three-dimensional MHD simulation. *Journal of Geophysical Research* 104 (A2). doi:10.1029/1998JA900080.6536.
- Kabin, K., Israelevich, P., Ershkovich, A., Neubauer, F., Gombosi, T., De Zeeuw, D., Powell, K., 2000. Interaction of the Saturnian magnetosphere with Titan: results of a three-dimensional MHD simulation. *Journal of Geophysical Research* 104 (A2). doi:10.1029/1998JA900080.6536.
- Kallio, E., Sillanpää, I., Janhunen, P., 2004. Titan in subsonic and supersonic flow. *Geophysical Research Letters* 31, L15703. doi:10.1029/2004GL020344.
- Kallio, E., Sillanpää, I., Jarvinen, R., Janhunen, P., Dougherty, M., Bertucci, C., Neubauer, F., 2007. Morphology of the magnetic field near Titan: hybrid model study of the Cassini T9 flyby. *Geophysical Research Letters* 34, L24509. doi:10.1029/2007GL030827.
- Keller, C.N., Cravens, T.E., 1994. One-dimensional multispecies hydrodynamic models of the wakeside ionosphere of Titan. *Journal of Geophysical Research* 99 (A4), 6527–6536.
- Koldoba, A.V., Romanova, M.M., Ustyugova, G.V., Lovelace, R.V.E., 2002. Three dimensional MHD simulation of accretion to an inclined rotator: the “cubed sphere” method. *Astrophysical Journal* 576, L53–L56.
- Ledvina, S.A., Cravens, T.E., 1998. A three-dimensional MHD model of plasma flow around Titan. *Planetary and Space Science* 46 (9/10), 1175–1191.
- Lipatov, A.S., 2002. The Hybrid Multiscale Simulation Technology: An Introduction with Application to Astrophysical and Laboratory Plasmas. Springer-Verlag, Berlin, Heidelberg, New York, pp. 1–403.
- Lipatov, A.S. Merging for particle-mesh complex particle kinetic modeling of the multiple plasma beams. *Journal of Computational Physics*, submitted for publication.
- Lipatov, A.S., Combi, M.R., 2006. Effects of kinetic processes in shaping Io's global plasma environment: a 3D hybrid model. *Icarus* 180 (2), 412–427.
- Lipatov, A.S., Motschmann, U., Bagdonat, T., 2002. 3-D hybrid simulation of the interaction of the solar wind with a weak comet. *Planetary and Space Science* 50, 403–411.
- Lipatov, A.S., Sauer, K., Baumgärtel, K., 1997. 2.5-D hybrid code simulation of the solar wind interaction with weak comets and related objects. *Advances in Space Research* 20 (2), 279.
- Lipatov, A.S., Sittler Jr., E.C., Hartle, R.E., Cooper, J.F., Simpson, D.G., 2011. Background and pickup ion velocity distribution dynamics in Titan's plasma environment: 3D hybrid simulation and comparison with CAPS T9 observations. *Advances in Space Research* 48, 1114–1125. doi:10.1016/j.asr.2011.05.026.
- Lipatov, A.S., Zank, G.P., Pauls, H.L., 1998. The interaction of neutral interstellar H with the heliosphere: a 2.5-D particle-mesh Boltzmann simulation. *Journal of Geophysical Research* 103 (A12), 29679.
- Ma, Y.-J., Nagy, A.F., Toth, G., Cravens, T.E., Russell, C.T., Gombosi, T.I., Wahlund, J.-E., Crary, F.J., Coates, A.J., Bertucci, C.L., Neubauer, F.M., 2007. 3D global multi-species Hall-MHD simulation of the Cassini T9 flyby. *Geophysical Research Letters* 34, L24510. doi:10.1029/2007GRL031627.
- Mankofsky, A., Sudan, R.N., Denavit, J., 1987. Hybrid simulation of ion beams in background plasma. *Journal of Computational Physics* 70, 89–116.
- Modolo, R., Chanteur, G.M., Wahlund, J.-E., Canu, P., Kurth, W.S., Gurnett, D., Matthews, A.P., Bertucci, C., 2007a. Plasma environment in the wake of Titan from hybrid simulation: a case study. *Geophysical Research Letters* 34, L24507. doi:10.1029/2007GL030489.
- Modolo, R., Wahlund, J.-E., Boström, R., Canu, P., Kurth, W.S., Gurnett, D., Lewis, G.R., Coates, A.J., 2007b. Far plasma wake of Titan from the RPWS observations: a case study. *Geophysical Research Letters* 34, L24504. doi:10.1029/2007GL030482.
- Modolo, R., Chanteur, G.M., 2008. A global hybrid model for Titan's interaction with the Kronian plasma: application to the Cassini TA flyby. *Journal of Geophysical Research* 113, A01310. doi:10.1029/2007JA012453.1238.
- Nagy, A.F., Liu, Y., Hansen, K.C., Kabin, K., Gombosi, T.I., Combi, M.R., De Zeeuw, D.L., Powell, K.G., Kliore, A.J., 2001. The interaction between the magnetosphere of Saturn and Titan's ionosphere. *Journal of Geophysical Research* 106, 6151–6160.
- Sauer, K., Lipatov, A.S., Baumgärtel, K., Dubinin, E., 1997. Solar wind-Pluto interaction revised. *Advances in Space Research* 20 (2), 295.
- Sauer, K., Bogdanov, A., Baumgärtel, K., Dubinin, E., 1996. Plasma environment of comet Wirtanen during its low-activity stage. *Planetary and Space Science* 44 (7), 715–729.
- Sillanpää, I., Kallio, E., Janhunen, P., Schmidt, W., Mursula, K., Vilpola, J., Tanskanen, P., 2006. Hybrid simulation study of ion escape at Titan for different orbital positions. *Advances in Space Research* 28, 799–805.
- Simon, S., Boesswetter, A., Bagdonat, T., Motschmann, U., 2007a. Physics of the ion composition boundary: a comparative 3-D hybrid simulation study of Mars and Titan. *Annals of Geophysics* 25, 99–115.
- Simon, S., Boesswetter, A., Bagdonat, T., Motschmann, U., Glassmeier, K.-H., 2006. Plasma environment of Titan: a 3-D hybrid simulation study. *Annals of Geophysics* 24, 1113–1135.

- Simon, S., Kleindienst, G., Boesswetter, A., Bagdonat, T., Motschmann, U., Glassmeier, K.-H., Schule, J., Bertucci, C., Dougherty, M., 2007b. Hybrid simulation of Titan's magnetic field signature during the Cassini T9 flyby. *Geophysical Research Letters* 34, L24S08. doi:10.1029/2007GL029967.
- Sittler Jr., E.C., Hartle, R.E., Vinäs, A.F., Johnson, R.E., Smith, H.T., Mueller-Wodarg, I., 2005. Titan interaction with Saturn's magnetosphere: Voyager 1 results revisited. *Journal of Geophysical Research* 110, A09302. doi:10.1029/2004JA010759.
- Sittler, E.C., Hartle, R.E., Bertucci, C., Coates, A., Cravens, T., Dandouras, I., Shemansky, D., 2009. Energy deposition processes in Titan's upper atmosphere and its induced magnetosphere. In: Brown, R.H., Lebreton, J.P., Waite, J.H. (Eds.), *Titan from Cassini–Huygens*, Springer, Dordrecht, Heidelberg, London, New York, pp. 393–455.
- Sittler, E.C., Hartle, R.E., Johnson, R.E., Cooper, J.F., Lipatov, A.S., Bertucci, C., Coates, A.J., Szego, K., Shappirio, M., Simpson, D.G., Wahlund, J.-E., 2010. Saturn's magnetospheric interaction with Titan as defined by Cassini encounters T9 and T18: new results. *Planetary and Space Science* 58, 327–350.
- Spencer, E., Patra, S., Andriyans, T., Ward, J., Barjatya, A., 2008. Electron density and electron neutral collision frequency in the ionosphere using plasma impedance probe measurements. *Journal of Geophysical Research* 113, A09305. doi:10.1029/2007JA013004.
- Stebbing, R.F., Smith, A.C.H., Ehrhardt, H., 1964. Charge transfer between oxygen atoms and O^+ and H^+ ions. *Journal of Geophysical Research* 69 (11), 2349–2355.
- Szego, K., Bebesi, Z., Bertucci, C., Coates, A.J., Crary, F., Erdos, G., Hartle, R.E., Sittler Jr., E.C., Young, D.T., 2007. Charged particle environment of Titan during the T9 flyby. *Geophysical Research Letters* 34, L24S03. doi:10.1029/2007GL030677.
- Tikhonov, A.N., Samarskii, A.A., 1963. *Equations of Mathematical Physics*. MacMillan, New York 765 pp.
- Umeda, T., Omura, Y., Matsumoto, H., 2001. An improved masking method for absorbing boundaries in electromagnetic particle simulations. *Computer Physics Communications* 137, 286–299.
- Winske, D., Wu, C.S., Li, Y.Y., Mou, Z.Z., Guo, S.Y., 1985. Coupling of newborn ions to the solar wind by electromagnetic instabilities and their interaction with the bow shock. *Journal of Geophysical Research* 90, 2713–2726.
- Yelle, R.V., Borggren, N., de la Haye, V., Kasprzak, W.T., Niemann, H.B., Müller-Wodarg, I., Waite Jr., J.H., 2006. The vertical structure of Titan's upper atmosphere from Cassini ion neutral mass spectrometer measurements. *Icarus* 182, 567–576.